

1 **Conserved interactions required for in vitro inhibition of the main**
2 **protease of severe acute respiratory syndrome coronavirus 2**
3 **(SARS-CoV-2)**

4 Alina Shitrit¹, Daniel Zaidman², Ori Kalid³, Itai Bloch⁴, Dvir Doron⁵, Tali Yarnizky⁶, Idit
5 Buch⁷, Idan Segev⁸, Efrat Ben-Zeev⁹, Elad Segev¹⁰ and Oren Kobiler^{1#}

6 ¹ - The Department of Clinical Microbiology and Immunology, Sackler School of
7 Medicine, Tel-Aviv University, Tel-Aviv, Israel

8 ² - Department of Organic Chemistry Weizmann Institute of Science, Rehovot, Israel

9 ³ - Pardes Hana, Israel

10 ⁴ - Biotechnology Department, MIGAL-Galilee Research Institute, Kiryat-Shmona,
11 Israel

12 ⁵ - Chemical & Computational Toxicology, Non-Clinical Development, Global R&D,
13 Teva Pharmaceutical Industries Ltd., Netanya, Israel

14 ⁶ - Tali Yarnizky Scientific Consulting, Maccabim-Reut, Israel

15 ⁷ - Emendo Biotherapeutics Ltd. Ness Ziona, Israel

16 ⁸ - Rishon-LeZion, Israel

17 ⁹ - The Nancy and Stephen Grand Israel National Center for Personalized Medicine,
18 Weizmann Institute of Science, Rehovot, Israel

19 ¹⁰ - Department of Applied Mathematics, Faculty of Science, Holon Institute of
20 Technology, Israel

21 [#] corresponding author: Oren Kobiler, Department of Clinical Microbiology and
22 Immunology, Sackler School of Medicine, Tel Aviv University, Tel Aviv, 69978 Israel

23 Phone 972-36406063, e-mail:okobiler@tauex.tau.ac.il

24 **Keywords:** SARS-CoV-2, Protease inhibitors, Repurposing, Virtual screen, Covalent
25 and non-covalent compounds

27 **Abstract**

28 The COVID-19 pandemic caused by the SARS-CoV-2 requires a fast development of
29 antiviral drugs. SARS-CoV-2 viral main protease (Mpro, also called 3C-like protease,
30 3CLpro) is a potential target for drug design. Crystal and co-crystal structures of the
31 SARS-CoV-2 Mpro have been solved, enabling the rational design of inhibitory
32 compounds. In this study we analyzed the available SARS-CoV-2 and the highly
33 similar SARS-CoV-1 crystal structures. We identified within the active site of the Mpro,
34 in addition to the inhibitory ligands' interaction with the catalytic C145, two key H-bond
35 interactions with the conserved H163 and E166 residues. Both H-bond interactions
36 are present in almost all co-crystals and are likely to occur also during the viral
37 polypeptide cleavage process as suggested from docking of the Mpro cleavage
38 recognition sequence. We screened *in silico* a library of 6,900 FDA-approved drugs
39 (ChEMBL) and filtered using these key interactions and selected 29 non-covalent
40 compounds predicted to bind to the protease. Additional screen, using DOCKovalent
41 was carried out on DrugBank library (11,414 experimental and approved drugs) and
42 resulted in 6 covalent compounds. The selected compounds from both screens were
43 tested *in vitro* by a protease activity inhibition assay. Two compounds showed activity
44 at the 50 μ M concentration range. Our analysis and findings can facilitate and focus
45 the development of highly potent inhibitors against SARS-CoV-2 infection.

46 **Introduction**

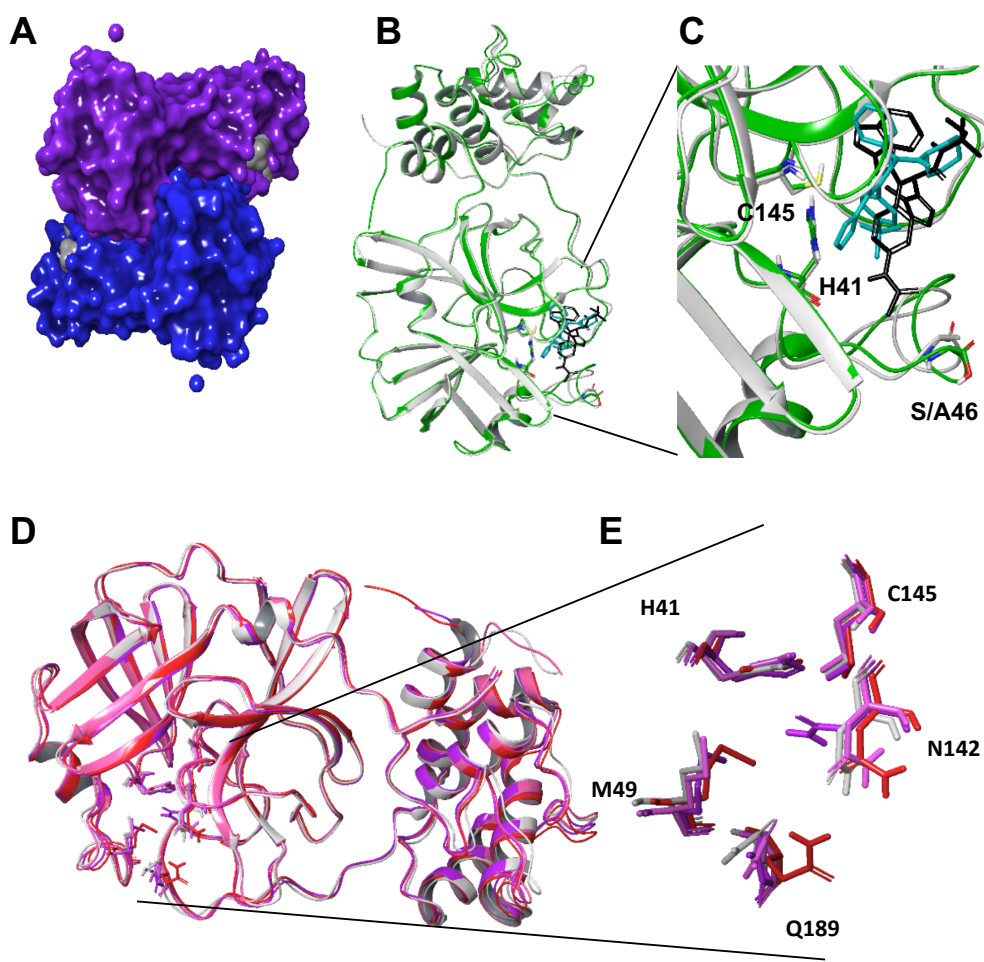
47 The raging pandemic caused by SARS-CoV-2 requires a rapid response of the
48 biomedical community^{1,2}. However, novel vaccines and antivirals require time for
49 development, thus repurposing of available drugs is a fast alternative and many
50 attempts using different approaches are made³⁻⁶. Antiviral drugs are traditionally
51 aimed at viral enzymes and are able to cure or reduce symptoms in several viral
52 infections (HIV, HCV and HSV-1⁷).

53 SARS-CoV-2, the causative agent of COVID-19, belongs to the genus
54 *Betacoronavirus* and is closely related to SARS-CoV-1, the causative agent of the
55 SARS pandemic outbreak in 2003⁸. Coronaviruses are unsegmented single-stranded
56 positive-stranded RNA viruses, featuring the largest known viral RNA genomes (26 to
57 32 kilobases in length) infecting humans⁹.

58 SARS-CoV-2 genome contains 14 open reading frames (ORFs) encoding 27 proteins.
59 First two ORFs at 5' untranslated region are coding for overlapping polyproteins
60 (replicase 1a (pp1a) and replicase 1ab (pp1ab)) approximately 450kD and 750kD,
61 respectively. The two polyproteins, pp1a and pp1ab, mediate all the functions required
62 for viral replication and transcription. The longer polyprotein (pp1ab) encodes for 15
63 nonstructural proteins (viral proteins that are not part of the virions) collectively
64 involved in virus replication and possibly in immune evasion.

65 The functional polypeptides are released from the polyproteins by extensive proteolytic
66 processing. This is primarily achieved by the main protease (Mpro), along with the
67 papain-like protease. Together, they cleave the amino acid backbone at 11 sites on
68 the large polyprotein. This cleavage site involves Leu-Gln↓(Ser/Ala/Gly) sequences

69 (the cleavage site is indicated by ↓)¹⁰. This cleavage pattern appears to be conserved
70 in the Mpro of SARS-CoV-1.



71

72 **Figure 1: Structural overview of main protease homodimer of SARS-CoV-2 and**
73 **its binding site. A.** Surface topology of SARS-CoV-2 Mpro homodimer in complex
74 with the covalent α -ketoamide inhibitor (PDB structure 6Y2F). The two monomers are
75 colored in blue and purple and the inhibitors are represented in gray. **B.**
76 Superimposition of SARS-CoV-2 Mpro (6W63, shown as ribbon and colored in green)
77 and SARS-CoV-1 (4MDS, shown as ribbon and colored in gray) in complex with their
78 non-covalent inhibitors X77 (shown as sticks and colored in blue) and ML300 (shown
79 as sticks and colored in black), respectively, shown as ribbons. The catalytic residues
80 H41 and C145 are in sticks. The different amino acids SARS-CoV-2 S46 and CoV-1
81 A46 are shown in sticks. **C.** Magnified view of Figure 1B (binding site) **D.**
82 Superimposition of the most diverse structures of SARS-CoV-2 and SARS-CoV-1
83 (available at that time) are shown in ribbons. SARS-CoV-1, 2ZU5 (gray), SFfARS-
84 CoV-2, 5R80 (purple), SARS-CoV-2, 6LU7 (pink), SARS-CoV-2, 6M03 (red), SARS-
85 CoV-2, 6Y2F (orange). Residues within this site Q189, M49 and N142 and the catalytic
86 residues H41 and C145 are represented in sticks. **E.** Magnified view of Figure 1D

87

88 The Mpro of the coronaviruses is a homodimer. It cleaves the polyprotein using its
89 catalytic dyad that contains the catalytic residues Histidine 41 (H41) and Cysteine 145
90 (C145) (Fig 1A-C). All of the residues within the active site, including the catalytic
91 residues and adjacent binding residues (polypeptide binding site) belong to one
92 monomer, except for one (Serine 1) from the second monomer¹¹.

93 Several co-crystal structures of the SARS-CoV-2 Mpro were recently solved, enabling
94 the rational design of specific inhibitory compounds¹²⁻¹⁵. The binding site of all the
95 ligands from the co-crystals is found within the Mpro active site. The close relationship
96 of SARS-CoV-2 to SARS-CoV-1 is reflected by high sequence identity of 96.1% and
97 similarity of 99% among their entire proteases protein sequence¹⁶. In the vicinity of the
98 binding site, the only residue that differs is positioned at residue 46. In SARS-CoV-2 it
99 is a Serine and in SARS-CoV-1 it is an Alanine; however, their side chains point out
100 of the binding site (Figure 1C).

101 The high similarity between the two viruses' proteins and the fact that their active sites
102 are practically identical, enable the use of SARS-CoV-1 co-crystals¹⁷⁻³⁴ in addition to
103 the available SARS-CoV-2 co-crystals, for understanding the vicinity of the binding site
104 region and defining the important interactions within the SARS-CoV-2 binding site with
105 its inhibitors. In this regard, it was suggested that drugs developed against SARS-
106 CoV-1 might be effective to treat SARS-CoV-2¹⁶. However, these compounds
107 remained in the preclinical or early clinical stage, without further development into an
108 approved medicine.

109 In this study, we analyzed the available SARS-CoV-1 and SARS-CoV-2 Mpro co-
110 crystal structures and the developed SARS-CoV-1 inhibitory compounds and identified

111 key interactions required to identify and develop an active inhibitor for the main
112 protease. We conducted a virtual screen using a library of only FDA-approved drugs
113 against SARS-CoV-2 Mpro structure from protein data bank (PDB) [6W63]¹³ using
114 three docking software tools (GOLD³⁵ and Glide³⁶⁻³⁸ and DOCKovalent³⁹). Several
115 compounds were selected and tested *in vitro* using a protease inhibition assay.

116 **Results**

117 **Analysis of co-crystals flexibility**

118 To identify the flexibility of the Mpro binding site, we superimposed the SARS-CoV-1
119 and SARS-CoV-2 apo and co-crystal structures available at the time of our study in
120 the PDB (Table 1). We selected the five most distinct, root-mean-square deviation
121 (RMSD)-wise, structures within the 3D space of the binding site. The selected
122 structures were 2ZU5, 5R80, 6LU7, 6M03, 6Y2F. Three flexible residues within the
123 binding site showed variation in their positions between the different structures:
124 Glutamine 189, Methionine 49 and Asparagine 142 (Figure 1D and E).

125 **Covalent and non-covalent co-crystal interactions**

126 To find the essential interactions required for inhibition of the SARS-CoV-2 Mpro, we
127 analyzed the interactions observed with both covalent and non-covalent inhibitors
128 (Table 1). Most of the co-crystals for SARS-CoV-1 and SARS-CoV-2 contain covalent
129 inhibitors (32 structures). To date, only 6 co-crystals contain non-covalent inhibitors.
130 Analyzing the co-crystal interactions of the non-covalent inhibitors revealed that the
131 two SARS-CoV-2 co-crystallized ligands, 3WL [6W63] and N3 [6M2N], form H-bonds
132 with protein NH donors: Histidine 163 (H163) and Glutamic acid 166 (E166) backbone.
133 Interestingly, N3 mediates the H-bond interaction with H163 through a water molecule
134 (Figure 2A). In SARS-CoV-1 co-crystals, three out of the four structures showed both
135 H163 and E166 backbone interactions and all exhibited the E166 backbone H-bond
136 interaction. Interestingly, F3F [2GZ8] mediates the E166 backbone interaction through
137 a water molecule.

Virus	Binding Type	Release date	Resolution	Ligand	Activity	PDB ID	H163	E166bb	Ref
SARS-CoV-2	non-covalent	03/2020	2.1 Å	X77		6W63	yes	yes	13
SARS-CoV-2	non-covalent	04/2020	1.56 Å	3WL		6M2N	yes*	yes	14
SARS-CoV-2	covalent	03/2020	1.95 Å	α-ketoamide 13b	IC50= 0.67μM	6Y2F	yes	yes	15
SARS-CoV-2	covalent	03/2020	2.2 Å	α-ketoamide 13b	IC50= 0.67μM	6Y2G	yes	yes	15
SARS-CoV-2	covalent	02/2020	2.16 Å	N3		6LU7	yes	yes	12
SARS-CoV-1	non-covalent	02/2013	1.6 Å	ML300/23H	IC50= 6.2μM	4MDS	yes	yes	29
SARS-CoV-1	non-covalent	08/2006	1.86 Å	D3F	IC50= 0.3μM	2GZ7	no	yes	26
SARS-CoV-1	non-covalent	08/2006	1.97 Å	F3F	IC50= 3μM	2GZ8	no	yes*	26
SARS-CoV-1	non-covalent	07/2007	1.80 Å	WR1	Ki= 2.2μM	2OP9	no	yes	20
SARS-CoV-1	non-covalent	01/2013	1.96 Å	0EN	IC50= 4.8μM	3V3M	yes	yes	21
SARS-CoV-1	covalent	03/2020	1.9 Å	OEW		6Y7M	yes	yes	32
SARS-CoV-1	covalent	06/2016	1.69 Å	SLH		5C5N	yes**	yes	27
SARS-CoV-1	covalent	06/2016	1.59 Å	SDJ		5C5O	yes	yes*	27
SARS-CoV-1	covalent	12/2012	1.95 Å	C4Z		3VB5	yes	yes	17
SARS-CoV-1	covalent	12/2012	2.5 Å	C6Z		3VB6	yes	yes	17
SARS-CoV-1	covalent	01/2009	1.65 Å	TG-0205486/ZU5	Ki= 0.099μM	2ZU5	yes	yes	22
SARS-CoV-1	covalent	01/2009	1.93 Å	TG-0204998/ZU3	Ki= 0.038μM	2ZU4	yes	yes	22
SARS-CoV-1	covalent	09/2005	1.85 Å	N9	Ki= 6.7μM	2AMD	yes	yes	30
SARS-CoV-1	covalent	09/2005	2.3 Å	N3		2AMQ	yes	yes	30
SARS-CoV-1	covalent	05/2006	1.93 Å	NOL	Ki= 0.053μM	2GX4	yes	yes	31
SARS-CoV-1	covalent	10/2005	1.88 Å	aza-peptide epoxide	Ki= 18μM	2A5I	yes	yes	23
SARS-CoV-1	covalent	08/2005	2.0 Å	N1	Ki= 10.7μM	1WOF	yes	yes	30
SARS-CoV-1	covalent	10/2005	2.3 Å	AZP	Ki= 18μM	2A5K	yes	yes	23
SARS-CoV-1	covalent	08/2006	1.9 Å	CY6	IC50= 70μM	2ALV	yes	yes	19
SARS-CoV-1	covalent	02/2008	1.9 Å	CYV	IC50= 80μM	2QIQ	yes	yes	18
SARS-CoV-1	covalent	12/2006	2.0 Å	AZP		2GTB	yes	yes	24
SARS-CoV-1	covalent	09/2011	1.99 Å	S89	Ki= 2.24μM	3SN8	no	yes	34
SARS-CoV-1	covalent	09/2011	1.89 Å	PRD_000 772	Ki= 8.27μM	3 SND	yes	no	34
SARS-CoV-1	covalent	07/2012	1.69 Å	G75		3SZN	yes	yes	33
SARS-CoV-1	covalent	08/2012	1.99 Å	G81		3TIT	yes	yes	33
SARS-CoV-1	covalent	08/2012	2.08 Å	G82		3TIU	yes	yes	33
SARS-CoV-1	covalent	09/2012	1.99 Å	G83		3TNS	yes	yes	33
SARS-CoV-1	covalent	09/2012	1.59 Å	G85		3TNT	yes	yes	33
SARS-CoV-1	covalent	02/2015	2.42 Å	3A7	IC50 = 63μM	4TWW	yes	th	28
SARS-CoV-1	covalent	02/2015	1.6 Å	3BL	IC50= 108μM	4TWY	yes	yes*	28
SARS-CoV-1	covalent	02/2015	1.89 Å	3X5	IC50= 240μM	4WY3	yes	no	28
SARS-CoV-1	covalent	03/2018	2.0 Å	8O5		5N5O	yes	yes	25
SARS-CoV-1	covalent	02/2018	1.62 Å	D03		5N19	yes	yes	25

139 **Table 1: SARS-CoV-1/2 Mpro covalent and non-covalent co-crystals PDB structures.** A list of all PDB structures used in this work and their interactions with the two key residues H163 and E166 backbone (bb) are summarized. The known activity

142 from the literature is mentioned when available in either inhibition concentration of 50%
143 (IC50) or inhibitory constant (Ki).

144 *-represent interaction through water molecule

145 **- introduces a donor to the imidazole

146 th-Theoretically represent interaction through water molecule, although the water
147 molecule is not present in the structure.

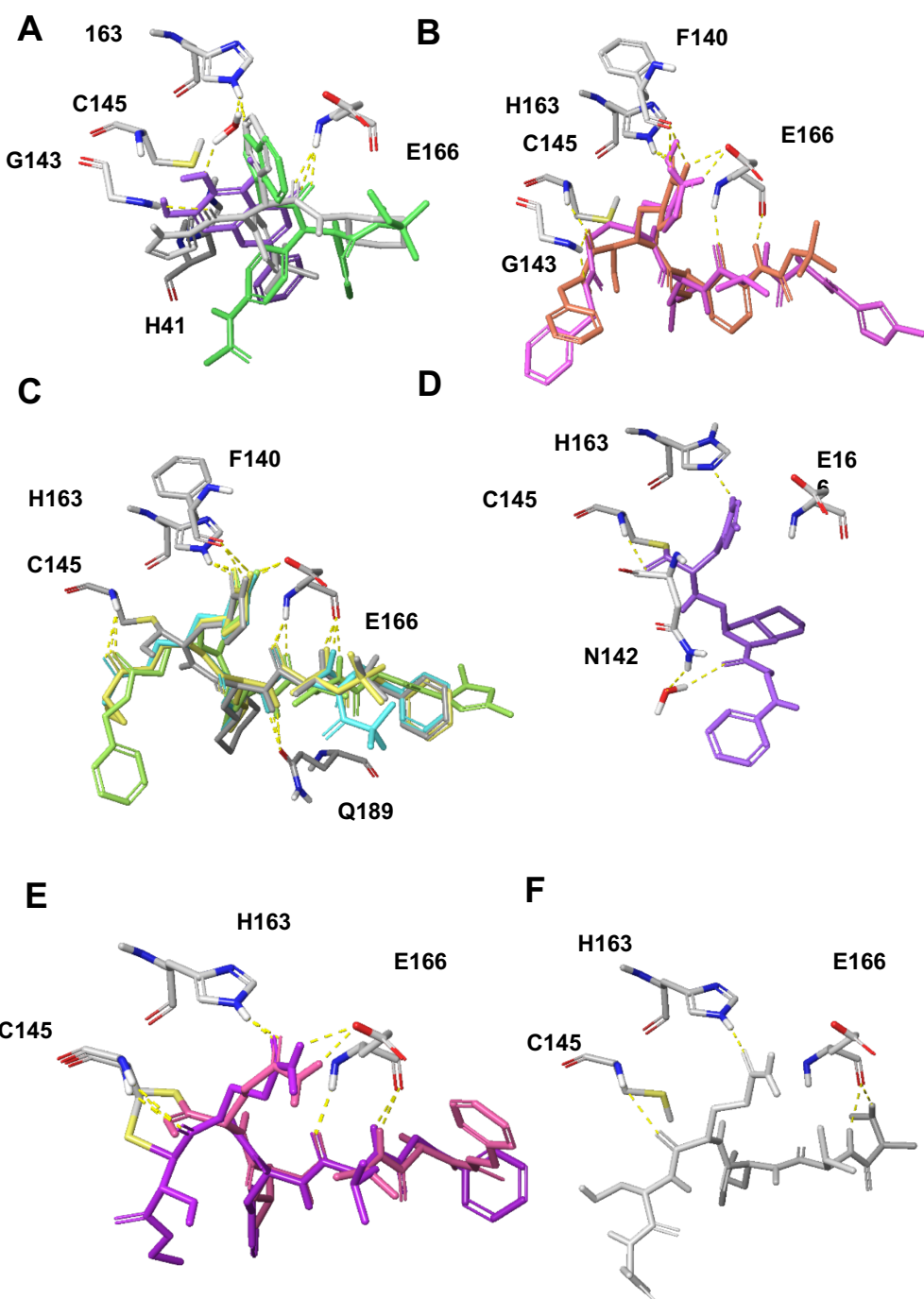
148

149 Additional interactions were observed with the following amino acids: The catalytic
150 H41 with D3F [2GZ7] and ML300 [4MDS]. The catalytic C145 forms a H-bond with
151 F3F [2GZ8]. G143 backbone with X77 [6W63] and N142 and F140 with F3F [2GZ8].
152 Many hydrophilic moieties of the ligands are surrounded by water molecules that
153 mediate the interaction of the inhibitor with the protein.

154 All covalent compounds interact with the catalytic C145 in the co-crystals.
155 Interestingly, most (31 out of 32) comprise also a non-covalent interaction, H-bond
156 with H163 similarly to the non-covalent compounds. All of the covalent and non-
157 covalent inhibitors present a H-bond acceptor to the side chain imidazole ring of H163
158 (see for example Figure 2A-C). The only exception, presenting a H-bond donor
159 towards H163, is SLH inhibitor [5C5N] (Figure 2D). Since the hydrogen can reside on
160 either nitrogen, (N1-H or N3-H tautomers) it interacts with the imidazole N acceptor.

161 E166 backbone that is interacting with all non-covalent ligands is also a key residue
162 for most covalent ligands. Most ligands (30 out of 32) form H-bond interactions with
163 the E166 backbone NH and some form an additional interaction with the E166
164 backbone carbonyl oxygen (for example, α -ketoamide 13b [6Y2F], ZU3 [2ZU4], N3
165 [2AMQ and 6LU7] and ZU5 [2ZU5], Figure 2B and C). Few structures mediate E166
166 backbone interaction through a water molecule (for example, F3F [4TWY] and SDJ

167 [5C5O]) (Table 1). In addition to E166 backbone interactions, some ligands interact
168 with E166 side chain either via salt bridge (for example, N3 [6LU7] and SLH [5C5N])
169 or through a H-bond interaction (for example, α -ketoamide 13b [6Y2F] and ZU3
170 [2ZU4], Fig 2B and 3C).



171

172 **Figure 2: Co-crystals interactions and important residues.** A. Superimposition of
173 non-covalent co-crystals 6W63 (gray), 4MDS (green) and 6M2N (purple) with protein

174 residues shown in sticks (colored by element). **B.** Superimposition of covalent co-
175 crystals 6LU7 (pink), 6Y2F (orange). **C.** Superimposition of covalent co-crystals 2GX4
176 (gray), 2ZU4 (cyan), 2AMQ (green), 2ZU5 (yellow), shown in sticks. **D.** 5C5N (purple),
177 shown in sticks. Protein interactions residues are in shown in sticks. **E.** Two co-crystals
178 with peptides 2A5I (purple), 3VB5 (pink). **F.** The recognition sequence peptide docked
179 within the 6LU7 (gray).

180

181 Other backbone interactions can be detected with G143 [6LU7, 6Y2F and 2ZU4],
182 H164 [6LU7] and F140 [2GX4 and 6LU7]. In addition, side chain interaction is formed
183 by ZU3 [2ZU4] with the flexible residue Q189 (Figures 2B and C).

184

185 **Docking of the cleavage recognition sequence**

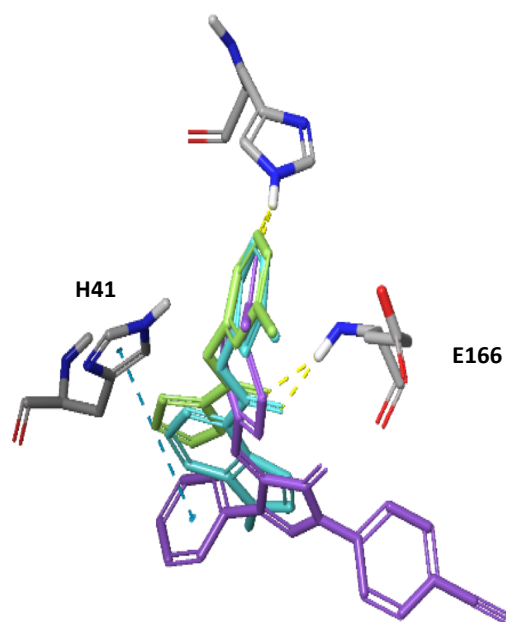
186 The proteolytic activity of Mpro catalyzes cleavage between Serine and Glutamine
187 within the viral polypeptides. To characterize the interactions required for cleavage,
188 we analyzed two co-crystals with peptidomimetic inhibitors [2A5I, 3VB5]. In these
189 structures, the side chain of the catalytic C145 binds the peptide Serine backbone.
190 The catalytic C145 side chain is rigid in all co-crystals except for [2A5I] in which the
191 side chain adopts a unique conformation. Interestingly, the peptide Glutamine side
192 chain of the cleavage site is anchored by a H-bond interaction with the H163 imidazole
193 (Fig 2E).

194 To characterize the interactions of the cleavage recognition sequence peptide we
195 chose, based on the peptidomimetic inhibitors, the following sequence: Ala, Val, Leu,
196 Gln, Ser, Ala, Gly. We docked (using Glide) the recognition sequence peptide to SARS
197 CoV-2 6LU7 crystal structure and superimposed the two co-crystals with the peptides
198 [2A5I, 3VB5]. The Glutamine within the recognition sequence adopted the same
199 conformation as in the two co-crystals, presenting the same H-bond interaction with

200 H163 imidazole (Fig 2F). In addition, the peptide's Valine and Alanine backbone
201 interact with the E166 backbone (through water molecules).

202 **Docking of known SARS-CoV-1 Mpro inhibitors**

203 Since the SARS-CoV-1 outbreak in 2003, several studies have developed inhibitors
204 for Mpro of SARS-CoV-1⁴⁰. To verify that our observed interactions are required for
205 Mpro inhibition, we docked non-covalent SARS-CoV-1 Mpro inhibitors to the SARS-
206 CoV-2 Mpro binding site [6W63]. The same two common interactions (H163 and E166)
207 were present in all compounds tested (see for example few known inhibitors in Figure
208 3).



209
210 **Figure 3:** SARS-CoV-1 developed inhibitor docked to Mpro 6W63 PDB structure.
211 Zhang2007 cmp37 (green), ghosh2008 cmp10 (cyan), Lu2006_Pyrazolone cmpd2p
212 (purple). Important residues for interactions are shown in sticks.

213
214 In summary, the two hydrophilic interactions with H163 and E166 backbone exist in
215 most of the covalent and non-covalent co-crystal ligands and all of these co-crystals

216 show at least one of these interactions. The known inhibitors show the same pattern
217 of interactions and these interactions seem to play a role in the recognition sequence
218 binding, thus highlighting them as biologically significant. Therefore, in the screening
219 process these interactions were chosen as filtering criteria, allowing to pass only poses
220 that satisfied at least one of these two interactions, for further analysis.

221 In addition, the Schrödinger SiteMap tool^{41,42} identified two hydrophobic regions within
222 the vicinity of the binding site and we found that most of the covalent and non-covalent
223 co-crystal ligands and the known inhibitors introduced hydrophobic moieties within
224 those regions.

225 **Non-covalent docking using GOLD and Glide**

226 To identify possible inhibitors from the FDA-approved drugs we used [6W63] protein
227 structure as a template for virtual screening, applying two docking software (as
228 recommended⁴³). The prepared ligand set originating from the ChEMBL drug
229 database was docked either using GOLD, outputting 10 conformations (poses) for
230 each compound resulting in 46,190 poses (3,634 unique drugs), or using Glide,
231 outputting at most 5 conformations (poses) per compound resulting in 22,004 poses
232 (3,620 unique drugs).

233 We filtered the poses based on the two significant interactions identified in our
234 analysis: H163 imidazole H-bond and E166 backbone amine H-bond (see the
235 Materials and Methods section for details). We chose the best docking poses that
236 satisfied either one or both of these interactions, resulting in at most three poses for
237 each compound. This stage resulted in 2,993 unique compounds poses in GOLD and
238 1,969 unique compounds in Glide. We manually selected the filtered poses resulting
239 in 21 compounds in GOLD and 13 in Glide. Altogether, a total of 29 unique compounds

240 (4 of which were selected in both methods) were selected and sent for assessment
241 using the protease inhibition assay. One compound, selected by the GOLD software,
242 GSK-256066, showed 37% inhibition at concentration of 50 μ M (Supplementary Table
243 1).

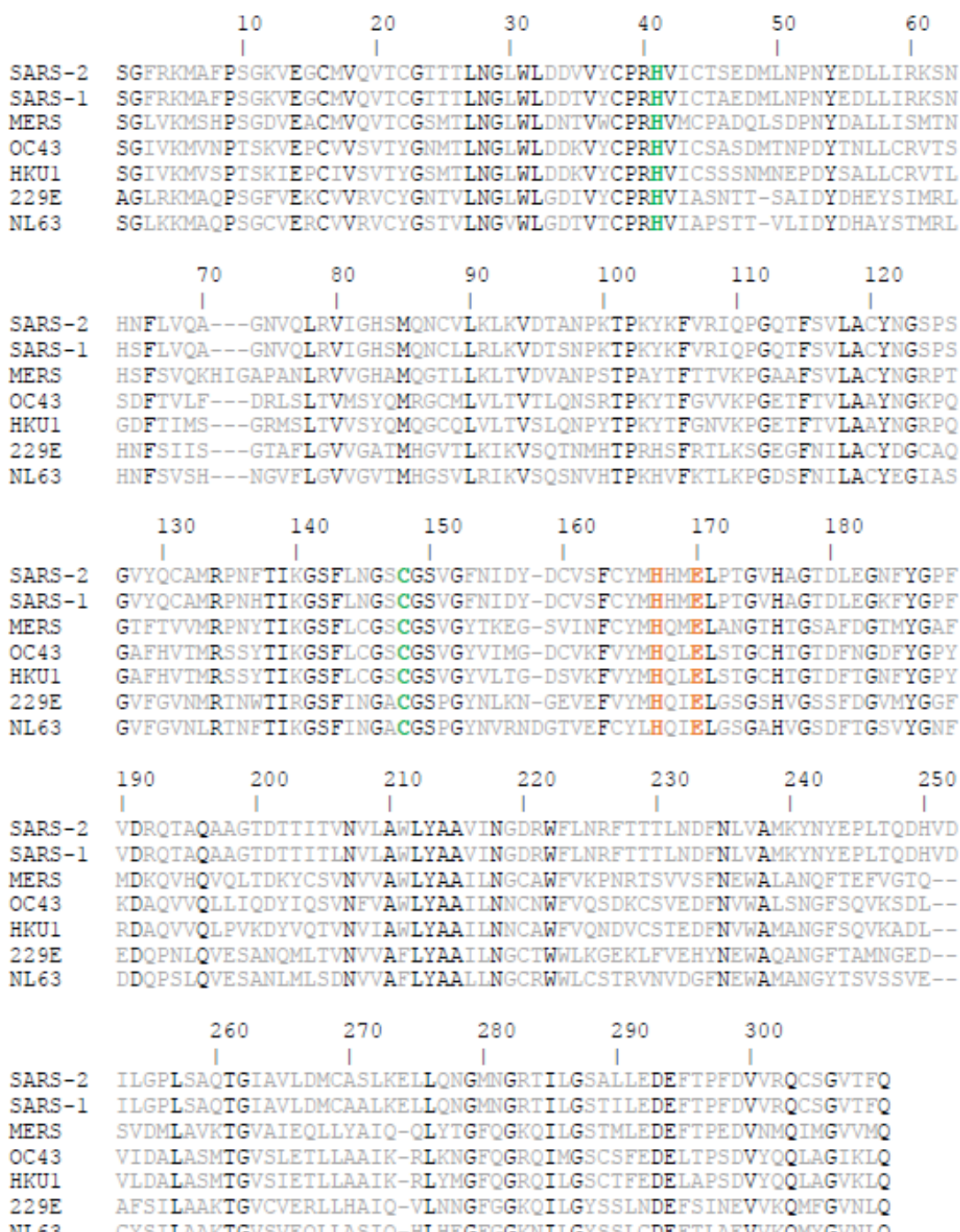
244 **Covalent docking using DOCKovalent**

245 Several covalent docking software were developed at Nir London's lab at the
246 Weizmann institute ³⁹. As there are very few possible known drugs that can perform
247 covalent binding, we used preclinical and clinical compounds from the DrugBank
248 database ⁴⁴. This database was filtered to contain only compounds with covalent
249 warheads that can be docked using DOCKovalent (see Materials and Methods) to:
250 [6M03, 5R7Y, 5R7Z, 6Y2F, 6W63, 4MDS, 2GX4, 6LU7] PDB structures. These
251 compounds were visually inspected and we selected the ones that showed additional
252 interactions to the C145 covalent interaction. We tested 5 nitriles and one Michael
253 acceptor and two of the nitriles (bicalutamide and ruxolitinib) showed 36% and 20%
254 inhibition at 50 μ M, respectively (Supplementary Table 2)

255 **Discussion**

256 Antiviral drugs targeting the Mpro of SARS-CoV-2 could support the fight against the
257 global COVID-19 pandemic. Here, to identify possible inhibitors of the SARS-CoV-2
258 Mpro, we have explored the co-crystal structures of the Mpro proteins of SARS-CoV-
259 2 and SARS-CoV-1. We identified two common interactions involving H163 and E166
260 that appeared in most co-crystals. We screened *in silico* drug databases for covalent
261 and non-covalent compounds. Possible compounds were further tested in a protease
262 inhibition assay and we found several compounds that reduce protease activity by
263 more than 30%.

264 The Mpro protein sequence of SARS-CoV-2 is highly similar (99%) to SARS-CoV-1.
265 In the region of the binding site only one residue is different. Some studies suggested
266 that the differences between the two proteins affected the ability to bind inhibitors^{45,46}.
267 On the other hand, several studies and our protease inhibition assay show that
268 inhibitors identified for SARS-CoV-1 Mpro also inhibit SARS-CoV-2 Mpro (see
269 Supplementary Table 3). Further co-crystals of SARS-CoV-1 [2MAQ] and SARS-CoV-
270 2 [6LU7] Mpro with the identical inhibitor (N3) show similar interactions with the
271 protease binding site¹². Thus, we inferred that the binding to the binding site of both
272 viruses is comparable and therefore we were able to analyze the key interactions
273 based on co-crystals obtained from both viruses.
274 We identified that all co-crystals have at least one of two key interactions with H163
275 and E166. Docking of the recognition sequence peptide into the binding site revealed
276 that H163 and E166 form H-bonds with the peptide. Specifically, the imidazole ring of
277 H163 interacts with the conserved Glutamine of the cleavage site¹¹ while E166
278 interacts with the Alanine and Valine from the recognition sequence. Interestingly,
279 E166 side chain interacts with Serine 1 NH₂-terminal of the second monomer^{11,47}. This
280 salt bridge interaction minimizes the conformational flexibility of E166 backbone and
281 assists in generating the correct orientation of the substrate binding site, which
282 explains the importance of dimerization for the catalytic activity⁴⁷. H163 and E166
283 amino acids are conserved among all human coronaviruses (2 alpha- and 5 beta-
284 coronaviruses Figure 4), unlike H164 and Q189 that were previously identified as
285 important interactions of several inhibitors^{12,22}. Thus, drugs developed to interact with
286 these amino acids may be effective against all human coronaviruses and could
287 potentially prevent the emergence of viral resistance.



288

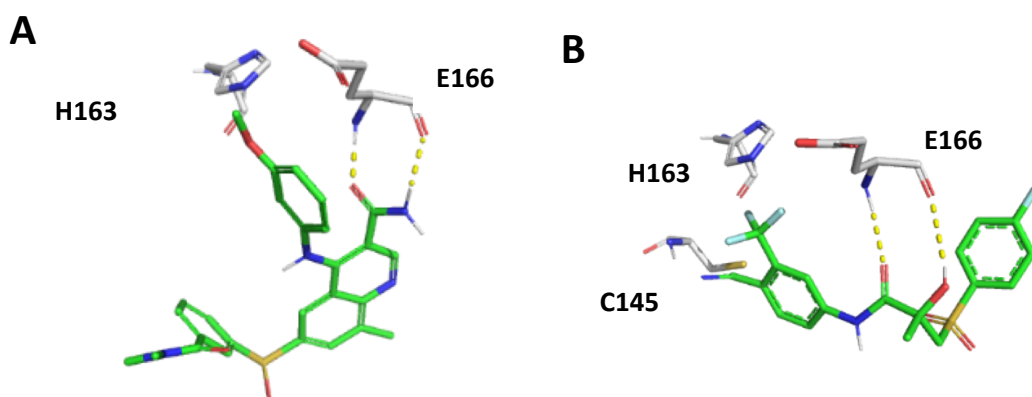
289 **Figure 4: Conservation of human coronaviruses Mpro.** Conserved residues are 290 colored in black. Specifically, catalytic dyad residues (H41 and C145) are colored in 291 green. H163 and E166 are colored in orange.

292

293 Several attempts to identify in-silico inhibitors of SARS-CoV-2 Mpro have been already 294 published⁴⁸⁻⁵². All of these did not validate their virtual screen results by in-vitro

295 experiments. Further, these studies used either [6LU7] or [6Y2F], as their template for
296 the computational screening. We used [6W63] as the protein structure for our non-
297 covalent docking, as [6W63] ligand is non-covalent while [6LU7] and [6Y2F] ligands
298 are covalent. The protein structure of [6W63] differs from [6LU7] and [6Y2F] in the
299 identified co-crystals flexibility residues M49, Q189 and N142 (Figure 1D and E). For
300 the covalent docking we used seven different crystal structures (see results) to allow
301 more flexibility in the binding site.

302 Our two screening analyses resulted in two clinically approved drugs that inhibit the
303 Mpro by over 30% in 50 μ M.: The first one is GSK-256066, a phosphodiesterase (PDE)
304 4 inhibitor⁵³ that was under development in phase 2 for the treatment of chronic
305 obstructive pulmonary disease (COPD), asthma and seasonal allergic rhinitis. It is
306 administered as an inhalation formulation (powder) and as an intranasal formulation
307 (nasal spray suspension). Our model suggests that GSK-256066 forms a H-bond with
308 H163 and additional two H-bonds with the amine and carbonyl of E166 backbone
309 (Figure 5). It inhibits the Mpro by 37% at a concentration of 50 μ M.



311 **Figure 5. FDA-approved drugs that inhibit Mpro.** A. GSK-256066 (colored by
312 element) B. Bicalutamide (colored by element). Important residues for interactions are
313 shown in gray element sticks.

314 Another drug that showed inhibition of the Mpro is bicalutamide, which was selected
315 from the covalent screening. It contains an aryl nitrile that can covalently bind to the
316 protein. Bicalutamide is an oral non-steroidal anti-androgen for prostate cancer. It is
317 comprised of a 50:50 racemic mixture of the (R)- and (S)-enantiomers. Bicalutamide
318 binds to the androgen receptor. Our model suggests that its nitrile group covalently
319 binds to C145 and forms two H-bonds with the amine and carbonyl of the E166
320 backbone (Figure 5). Bicalutamide was tested in two experiments and inhibited Mpro
321 by 37% and 33% at a concentration of 50 μ M.

322 Several compounds that were previously identified as inhibitors with sub-micromolar
323 potency were active in our protease inhibition assay (Supplementary Table 3). Two of
324 these inhibitors with known sub-micromolar activity, showed limited inhibition (39%
325 and 9%) at a concentration of 50 μ M in our protease activity assay (Supplementary
326 Table 3). Thus, GSK-256066 and bicalutamide, that were identified in our protease
327 inhibition assay, have a similar inhibitory activity at the same concentration. These
328 results suggest that more assays should be conducted to test repurposing of these
329 drugs as anti-SARS therapeutics.

330 In conclusion, our analysis of the structural constraints required for the inhibition of
331 SARS-CoV-2 Mpro has suggested key interactions with several amino acids in the
332 active pocket of the protein. We were able to identify several approved drugs with a
333 potential to inhibit Mpro activity, indicating that our analysis could be used for virtual
334 screenings and rational drug development.

335

336 **Materials and Methods**

337 **Protein data bank (PDB) search**

338 The protein data bank was searched for SARS-CoV/SARS-CoV-1/SARS-CoV-2 Mpro.

339 Non SARS-CoV structures and non-human SARS-CoV like structures were omitted.

340 Co-crystals binding fragments were not added to this analysis due to their non-drug

341 like structures. We anticipate that few of the available structures might be overlooked

342 using these search criteria. All PDB structures found and analyzed are mentioned in

343 Table 1. Throughout the text, PDB IDs are marked with square brackets.

344 **Preparing a drug library from ChEMBL for non-covalent docking**

345 The ChEMBL database contains 6,900 drugs in various stages of clinical trials. To

346 focus our computational screen, the following filters were applied: small molecules that

347 were at clinical phase 2 or higher, number of rotatable bonds < 14, MW freebase 200-

348 990, ATC Class Level 1: all except D-Dermatologics and V-Various. This filtering

349 resulted in a 4,239-compound library. To prepare the ligands for docking simulations,

350 LigPrep (Schrödinger Release 2020-1: LigPrep, Schrödinger, LLC, New York, NY,

351 2020) was applied on the exported library. The following settings were used: (a) The

352 OPLS3e force field was chosen⁵⁴; (b) Possible protonation states were generated

353 using Ionizer at a target pH of 7.4 ; (c) All ligands were desalted; (d) No tautomers

354 were generated; (e) At most two stereoisomeric forms were produced per ligand for

355 unspecified chiral centers. These constraints enabled us to expand the initial 4,239-

356 compound library to only 4,623 ligands.

357 **Preparing a drug library from DrugBank for covalent docking**

358 We used the DrugBank database⁴⁴ that includes 11414 preclinical and clinical small

359 molecules. These compounds were filtered by ≤500D MW and ≤5 rotatable bonds.

360 Only compounds that contain covalent warheads (Michael acceptors:
361 O=CC=[C;H1,H2] or nitriles) were selected as they can covalently bind the thiol of
362 C145. The filtering resulted in a library of 437 ligands (258 Michael acceptors and 179
363 nitriles).

364 **Docking**

365 The 4,623 prepared ligands originating from ChEMBL were docked using Glide
366 (Schrödinger Release 2020-1: Glide, Schrödinger, LLC, New York, NY, 2020) to the
367 Mpro structure from [6W63], keeping the protein structure rigid and ligands flexible,
368 with no constraints applied on specific receptor-ligand hydrogen bond (H-bond)
369 interactions. The standard precision (SP) mode of Glide was used based on the
370 OPLS3e force field, writing out at most 5 poses per ligand. The 22,003 conformations
371 (poses) were filtered by requiring at least one of the two key H-bond interactions with
372 H163 and E166. The default maximum H-bond distance criterion of 2.5 Å was
373 stretched to 3.0 Å. This filter resulted in three groups of poses: (a) 517 poses
374 interacting with both H163 and E166; (b) 2,088 poses forming a H-bond with H163
375 only; and (c) 2,678 poses forming a H-bond with E166 only. In each of the filtered
376 groups, the pose with the best Glide score per each ligand was selected, resulting in
377 293, 879 and 1,347 poses, respectively. We further narrowed down the number of
378 poses by eliminating drugs with molecular charge below -1 using Maestro's Ligand
379 Filtering utility. Applying this filter resulted in 260, 820 and 1,283 poses, respectively.
380 Removing the duplicate poses (i.e. those overlapping with one associated with either
381 or both of the two other groups) resulted in a total of 1,969 unique poses.
382 The 4,239 ChEMBL-derived (“pre-Ligprep”) drugs were also docked using GOLD
383 Standard docking³⁵ to Mpro structure from [6W63] resulting in 46,190 poses (10 poses

384 per ligand). Identical filters as in Glide docking were applied resulting in a total of 2,993
385 unique poses that were grouped by interactions to (a) 86 poses interacting with both
386 H163 and E166; (b) 1,011 poses forming H-bond with H163 only; and (c) 1,896 poses
387 forming H-bond with E166 only.

388 **Selection**

389 In our manual selection we preferred ligands that in addition to one or two important
390 interactions (H163 and E166) also formed interactions with additional residues that
391 were found in the co-crystal structure (for example Gly143 backbone). In addition, we
392 favored compounds that did not violate the two hydrophobic regions within the binding
393 site as calculated by Maestro's SiteMap tool (Schrödinger Release 2020-1: SiteMap,
394 Schrödinger, LLC, New York, NY, 2020.^{41,42}).

395 **Protease inhibitor activity assay**

396 35 compounds were obtained as detailed in Supplementary Table 1 and 2. The
397 compounds were prepared in assay ready plates (Greiner 784900) using Labcyte
398 Echo 555 and diluted in DMSO to concentration of 0.5%. 5nM Mpro and 375nM [5-
399 FAM]-AVLQSGFR-[Lys(Dabcyl)-K-amide substrate (in 20mM HEPES pH=7.3, 50mM
400 NaCl, 10% Glycerol, 0.01% Tween-20, 1mM TCEP) were added to the compounds
401 and incubated for 30 minutes at room temperature. Fluorescence was read at 480/520
402 ex/em in BMG Pherastar FS.

403 The Mpro inhibition assay was carried out in the Mantoux Bioinformatics institute of
404 the Nancy and Stephen Grand Israel National Center for Personalized Medicine
405 (INCPM), Weizmann Institute of Science.

406

407 **Funding**

408 This work was supported by grants from the Israel Science foundation (grant
409 #1387/14) to O.K. The funders had no role in study design, data collection and
410 analysis, decision to publish, or preparation of the manuscript.

411 **Author Contributions**

412 AS and OKo designed research; AS, DZ, OKa, IB, DD, TY, IB, IS, EBZ and ES
413 analyzed data; AS, DZ, OKa, IB, DD, TY, IB, IS, EBZ and ES performed research;
414 AS and OKo wrote the paper.

415 **Acknowledgement**

416 We thank Craig Coel and Katalin Phimister from Schrödinger for all their support, Haim
417 Barr and Nir London for their help and all Kobiler lab members for their comments.

418 **Supplementary Table Legends**

419 **Supplementary Table 1: Non-covalent compounds that were selected for testing**
420 **and their % of inhibition at 50µM concentration.** A list of all non-covalent
421 compounds tested in the protease inhibition assay after selection either by the GOLD,
422 Glide or both docking tools. Percent average inhibition at 50µM is presented (Avg.
423 Inh).

424 **Supplementary Table 2: Covalent compounds that were selected for testing and**
425 **their % of inhibition at 50µM concentration.** A list of all covalent compounds tested
426 in the protease inhibition assay after selection. Percent average inhibition at 50µM is
427 presented (Avg. Inh).

428 **Supplementary Table 3: Several SARS-CoV-1 known Mpro inhibitors and their**
429 **results in the protease inhibition assay.** The structures (column A) and activity
430 Column C) of several SARS-CoV-1 inhibitors are known from the publications (column
431 D) along with the results obtained in our protease inhibition assay (columns E-H).

432

433 **References**

434 1 Sohrabi, C. *et al.* World Health Organization declares global emergency: A review of
435 the 2019 novel coronavirus (COVID-19). *Int J Surg* **76**, 71-76,
436 doi:10.1016/j.ijsu.2020.02.034 (2020).

437 2 Wang, C., Horby, P. W., Hayden, F. G. & Gao, G. F. A novel coronavirus outbreak of
438 global health concern. *Lancet* **395**, 470-473, doi:10.1016/S0140-6736(20)30185-9
439 (2020).

440 3 Weston, S. *et al.* Broad anti-coronaviral activity of FDA approved drugs against SARS-
441 CoV-2 in vitro and SARS-CoV in vivo. *bioRxiv*, 2020.2003.2025.008482,
442 doi:10.1101/2020.03.25.008482 (2020).

443 4 Saul, S. & Einav, S. Old drugs for a new virus: repurposed approaches for combating
444 COVID-19. *ACS Infect Dis*, doi:10.1021/acsinfecdis.0c00343 (2020).

445 5 Riva, L. *et al.* Discovery of SARS-CoV-2 antiviral drugs through large-scale compound
446 repurposing. *Nature*, doi:10.1038/s41586-020-2577-1 (2020).

447 6 Panda, P. K. *et al.* Structure-based drug designing and immunoinformatics approach
448 for SARS-CoV-2. *Sci Adv* **6**, eabb8097, doi:10.1126/sciadv.eabb8097 (2020).

449 7 Muller, B. & Krausslich, H. G. Antiviral strategies. *Handb Exp Pharmacol*, 1-24,
450 doi:10.1007/978-3-540-79086-0_1 (2009).

451 8 Chan, J. F. *et al.* Genomic characterization of the 2019 novel human-pathogenic
452 coronavirus isolated from a patient with atypical pneumonia after visiting Wuhan.
453 *Emerg Microbes Infect* **9**, 221-236, doi:10.1080/22221751.2020.1719902 (2020).

454 9 Howley, P. M. & Knipe, D. M. *Fields Virology - Emerging Viruses*. (Lippincott
455 Williams & Wilkins, 2020).

456 10 Ziebuhr, J., Snijder, E. J. & Gorbatenko, A. E. Virus-encoded proteinases and
457 proteolytic processing in the Nidovirales. *J Gen Virol* **81**, 853-879, doi:10.1099/0022-
458 1317-81-4-853 (2000).

459 11 Yang, H. *et al.* The crystal structures of severe acute respiratory syndrome virus main
460 protease and its complex with an inhibitor. *Proc Natl Acad Sci USA* **100**, 13190-13195,
461 doi:10.1073/pnas.1835675100 (2003).

462 12 Jin, Z. *et al.* Structure of M(pro) from SARS-CoV-2 and discovery of its inhibitors.
463 *Nature* **582**, 289-293, doi:10.1038/s41586-020-2223-y (2020).

464 13 Mesecar, A. D. A taxonomically-driven approach to development of potent, broad-
465 spectrum inhibitors of coronavirus main protease including SARS-CoV-2 (COVID-
466 19). <http://www.rcsb.org/structure/6W63>, doi:10.2210/pdb6w63/pdb [doi].

467 14 Su, H. X., Yao, S., Zhao, W.F., Li, M.J., Zhang, L.K., Ye, Y., Jiang, H.L., Xu, Y.C.
468 Identification of a novel inhibitor of SARS-CoV-2 3CLpro.
<http://www.rcsb.org/structure/6M2N>, doi:10.2210/pdb6m2n/pdb [doi].

469 15 Zhang, L. *et al.* Crystal structure of SARS-CoV-2 main protease provides a basis for
470 design of improved alpha-ketoamide inhibitors. *Science*, doi:10.1126/science.abb3405
471 (2020).

472 16 Xu, Z. *et al.* Nelfinavir was predicted to be a potential inhibitor of 2019-nCoV main
473 protease by an integrative approach combining homology modelling, molecular
474 docking and binding free energy calculation. *bioRxiv*, 2020.2001.2027.921627,
475 doi:10.1101/2020.01.27.921627 (2020).

476 17 Chuck, C. P. *et al.* Design, synthesis and crystallographic analysis of nitrile-based
477 broad-spectrum peptidomimetic inhibitors for coronavirus 3C-like proteases. *Eur J
478 Med Chem* **59**, 1-6, doi:10.1016/j.ejmech.2012.10.053 (2013).

480 18 Ghosh, A. K. *et al.* Structure-based design, synthesis, and biological evaluation of
481 peptidomimetic SARS-CoV 3CLpro inhibitors. *Bioorg Med Chem Lett* **17**, 5876-5880,
482 doi:10.1016/j.bmcl.2007.08.031 (2007).

483 19 Ghosh, A. K. *et al.* Design and synthesis of peptidomimetic severe acute respiratory
484 syndrome chymotrypsin-like protease inhibitors. *J Med Chem* **48**, 6767-6771,
485 doi:10.1021/jm050548m (2005).

486 20 Goetz, D. H. *et al.* Substrate specificity profiling and identification of a new class of
487 inhibitor for the major protease of the SARS coronavirus. *Biochemistry* **46**, 8744-8752,
488 doi:10.1021/bi0621415 (2007).

489 21 Jacobs, J. *et al.* Discovery, synthesis, and structure-based optimization of a series of N-
490 (tert-butyl)-2-(N-arylamido)-2-(pyridin-3-yl) acetamides (ML188) as potent
491 noncovalent small molecule inhibitors of the severe acute respiratory syndrome
492 coronavirus (SARS-CoV) 3CL protease. *J Med Chem* **56**, 534-546,
493 doi:10.1021/jm301580n (2013).

494 22 Lee, C. C. *et al.* Structural basis of inhibition specificities of 3C and 3C-like proteases
495 by zinc-coordinating and peptidomimetic compounds. *J Biol Chem* **284**, 7646-7655,
496 doi:10.1074/jbc.M807947200 (2009).

497 23 Lee, T. W. *et al.* Crystal structures of the main peptidase from the SARS coronavirus
498 inhibited by a substrate-like aza-peptide epoxide. *J Mol Biol* **353**, 1137-1151,
499 doi:10.1016/j.jmb.2005.09.004 (2005).

500 24 Lee, T. W. *et al.* Crystal structures reveal an induced-fit binding of a substrate-like Aza-
501 peptide epoxide to SARS coronavirus main peptidase. *J Mol Biol* **366**, 916-932,
502 doi:10.1016/j.jmb.2006.11.078 (2007).

503 25 Lin, D., Zhang, L., Kusov, Y., Nian, Y., Ma, Q., Wang, J., Leyssen, P., Lanko, K.,
504 Neyts, J., de Wilde, A., Snijder, E.J., Liu, H., Hilgenfeld, R. Alpha-ketoamides as
505 broad-spectrum inhibitors of coronavirus and enterovirus replication.
<http://www.rcsb.org/structure/5N5O>, doi:10.2210/pdb5n5o/pdb [doi].

506 26 Lu, I. L. *et al.* Structure-based drug design and structural biology study of novel
507 nonpeptide inhibitors of severe acute respiratory syndrome coronavirus main protease.
508 *J Med Chem* **49**, 5154-5161, doi:10.1021/jm060207o (2006).

509 27 Shimamoto, Y., Hattori, H., Kobayashi, K., Teruya, K., Sanjho, A., Nakagawa, A.,
510 Yamashita, E., Akaji, K. Fused-ring structure of N-decalin as a novel scaffold for SARS
511 3CL protease inhibitors. <http://www.rcsb.org/structure/5C5N>,
512 doi:10.2210/pdb5c5n/pdb [doi].

513 28 Shimamoto, Y. *et al.* Fused-ring structure of decahydroisoquinolin as a novel scaffold
514 for SARS 3CL protease inhibitors. *Bioorg Med Chem* **23**, 876-890,
515 doi:10.1016/j.bmcl.2014.12.028 (2015).

516 29 Turlington, M. *et al.* Discovery of N-(benzo[1,2,3]triazol-1-yl)-N-
517 (benzyl)acetamido)phenyl carboxamides as severe acute respiratory syndrome
518 coronavirus (SARS-CoV) 3CLpro inhibitors: identification of ML300 and noncovalent
519 nanomolar inhibitors with an induced-fit binding. *Bioorg Med Chem Lett* **23**, 6172-
520 6177, doi:10.1016/j.bmcl.2013.08.112 (2013).

521 30 Yang, H. *et al.* Design of wide-spectrum inhibitors targeting coronavirus main
522 proteases. *PLoS Biol* **3**, e324, doi:10.1371/journal.pbio.0030324 (2005).

523 31 Yang, S. *et al.* Synthesis, crystal structure, structure-activity relationships, and antiviral
524 activity of a potent SARS coronavirus 3CL protease inhibitor. *J Med Chem* **49**, 4971-
525 4980, doi:10.1021/jm0603926 (2006).

526 32 Zhang, L., Lin, D., Hilgenfeld, R. Crystal structure of the complex resulting from the
527 reaction between the SARS-CoV main protease and tert-butyl (1-((S)-3-cyclohexyl-1-
528 (((S)-4-(cyclopropylamino)-3,4-dioxo-1-((S)-2-oxopyrrolidin-3-yl)butan-2-yl)amino)-

529

530 1-oxopropan-2-yl)-2-oxo-1,2-dihydropyridin-3-yl)carbamate.
531 <http://www.rcsb.org/structure/6Y7M>, doi:10.2210/pdb6y7m/pdb [doi].

532 33 Zhu, L., Hilgenfeld, R. Crystal structures of SARS-CoV main protease complexed with
533 a series of unsaturated esters. <http://www.rcsb.org/structure/3SZN>,
534 doi:10.2210/pdb3szn/pdb [doi].

535 34 Zhu, L. *et al.* Peptide aldehyde inhibitors challenge the substrate specificity of the
536 SARS-coronavirus main protease. *Antiviral Res* **92**, 204-212,
537 doi:10.1016/j.antiviral.2011.08.001 (2011).

538 35 Jones, G., Willett, P., Glen, R. C., Leach, A. R. & Taylor, R. Development and
539 validation of a genetic algorithm for flexible docking. *J Mol Biol* **267**, 727-748,
540 doi:10.1006/jmbi.1996.0897 (1997).

541 36 Friesner, R. A. *et al.* Glide: a new approach for rapid, accurate docking and scoring. 1.
542 Method and assessment of docking accuracy. *J Med Chem* **47**, 1739-1749,
543 doi:10.1021/jm0306430 (2004).

544 37 Friesner, R. A. *et al.* Extra precision glide: docking and scoring incorporating a model
545 of hydrophobic enclosure for protein-ligand complexes. *J Med Chem* **49**, 6177-6196,
546 doi:10.1021/jm0512560 (2006).

547 38 Halgren, T. A. *et al.* Glide: a new approach for rapid, accurate docking and scoring. 2.
548 Enrichment factors in database screening. *J Med Chem* **47**, 1750-1759,
549 doi:10.1021/jm030644s (2004).

550 39 London, N. *et al.* Covalent docking of large libraries for the discovery of chemical
551 probes. *Nat Chem Biol* **10**, 1066-1072, doi:10.1038/nchembio.1666 (2014).

552 40 Wu, C. Y. *et al.* Stable benzotriazole esters as mechanism-based inactivators of the
553 severe acute respiratory syndrome 3CL protease. *Chem Biol* **13**, 261-268,
554 doi:10.1016/j.chembiol.2005.12.008 (2006).

555 41 Halgren, T. New method for fast and accurate binding-site identification and analysis.
556 *Chem Biol Drug Des* **69**, 146-148, doi:10.1111/j.1747-0285.2007.00483.x (2007).

557 42 Halgren, T. A. Identifying and characterizing binding sites and assessing druggability.
558 *J Chem Inf Model* **49**, 377-389, doi:10.1021/ci800324m (2009).

559 43 Chaput, L., Martinez-Sanz, J., Saettel, N. & Mouawad, L. Benchmark of four popular
560 virtual screening programs: construction of the active/decoy dataset remains a major
561 determinant of measured performance. *J Cheminform* **8**, 56, doi:10.1186/s13321-016-
562 0167-x (2016).

563 44 Wishart, D. S. *et al.* DrugBank 5.0: a major update to the DrugBank database for 2018.
564 *Nucleic Acids Res* **46**, D1074-D1082, doi:10.1093/nar/gkx1037 (2018).

565 45 Bzowka, M. *et al.* Structural and Evolutionary Analysis Indicate That the SARS-CoV-
566 2 Mpro Is a Challenging Target for Small-Molecule Inhibitor Design. *Int J Mol Sci* **21**,
567 doi:10.3390/ijms21093099 (2020).

568 46 Krishnamoorthy, N. Variable Structural Networks at the Active Site of the SARS-CoV
569 and SARS-CoV2 Main Proteases. *Preprints* **2020030423**, doi:
570 10.20944/preprints202003.0423.v1 (2020).

571 47 Goyal, B. & Goyal, D. Targeting the Dimerization of the Main Protease of
572 Coronaviruses: A Potential Broad-Spectrum Therapeutic Strategy. *ACS Comb Sci* **22**,
573 297-305, doi:10.1021/acscombsci.0c00058 (2020).

574 48 Choudhary, M. I., Shaikh, M., Tul-Wahab, A. & Ur-Rahman, A. In silico identification
575 of potential inhibitors of key SARS-CoV-2 3CL hydrolase (Mpro) via molecular
576 docking, MMGBSA predictive binding energy calculations, and molecular dynamics
577 simulation. *PLoS One* **15**, e0235030, doi:10.1371/journal.pone.0235030 (2020).

578 49 Elmezayen, A. D., Al-Obaidi, A., Sahin, A. T. & Yelekci, K. Drug repurposing for
579 coronavirus (COVID-19): in silico screening of known drugs against coronavirus 3CL

580 hydrolase and protease enzymes. *J Biomol Struct Dyn*, 1-13,
 581 doi:10.1080/07391102.2020.1758791 (2020).

582 50 Hage-Melim, L. *et al.* Virtual screening, ADME/Tox predictions and the drug
 583 repurposing concept for future use of old drugs against the COVID-19. *Life Sci* **256**,
 584 117963, doi:10.1016/j.lfs.2020.117963 (2020).

585 51 Mittal, L., Kumari, A., Srivastava, M., Singh, M. & Asthana, S. Identification of
 586 potential molecules against COVID-19 main protease through structure-guided virtual
 587 screening approach. *J Biomol Struct Dyn*, 1-19, doi:10.1080/07391102.2020.1768151
 588 (2020).

589 52 Wu, C. *et al.* Analysis of therapeutic targets for SARS-CoV-2 and discovery of
 590 potential drugs by computational methods. *Acta Pharm Sin B*,
 591 doi:10.1016/j.apsb.2020.02.008 (2020).

592 53 Tralau-Stewart, C. J. *et al.* GSK256066, an exceptionally high-affinity and selective
 593 inhibitor of phosphodiesterase 4 suitable for administration by inhalation: in vitro,
 594 kinetic, and in vivo characterization. *J Pharmacol Exp Ther* **337**, 145-154,
 595 doi:10.1124/jpet.110.173690 (2011).

596 54 Harder, E. *et al.* OPLS3: A Force Field Providing Broad Coverage of Drug-like Small
 597 Molecules and Proteins. *J Chem Theory Comput* **12**, 281-296,
 598 doi:10.1021/acs.jctc.5b00864 (2016).

599